Validation of the Proposed Analytical Method

4.1 Introduction

Fabrication of RFSMPM and AFSMPM machines has been discussed in previous Chapter and their operation using PM Enhanced sensing scheme with shadow coil using experimental results obtained from prototypes developed, the details of which has been given in Table 3.1. Section 4.2 discusses the results obtained from Machine-A, a RFPM motor while section 4.3 discusses the results from AFPM motor; Machine-B, Machine-C and Machine-D. The analytical validation of the proposed method using published results and comparison of experimental results with different analysis methods has been accomplished in Section 4.4. The fault-tolerant characteristics of the two five-phase AFPM motors are studied in Section 4.5. The performance of these two motors has been compared. The Chapter is concluded in Section 4.6.

A typical drive characteristic for a PM motor has been shown in Fig. 4.1. For SMPM motors, the constant power region is short and can be extended by including flux weakening control [Jang *et al.*, 2008; Sudhoff *et al.*, 1995; Song *et al.*, 1996].

4.2 Radial Flux SMPM Motor: Machine-A

The experimental validation of the analytical results obtained from Machine-A has been validated with the experimental results as depicted in Fig. 4.2. The experimental and computed results obtained from Residue Theorem and Parseval's Theorem with isotropic and anisotropic models are compared. The anisotropic model considers the effect of stator slotting on the performance of the SMPM motors.

For constant voltage analysis current has been calculated as,

$$V = RI_1 + E \tag{4.1}$$

where, E is the speed induced back-EMF induced in the stator windings calculated as,

$$E = k_e \omega \tag{4.2}$$

The analytically computed results are compared with that obtained experimentally for constant voltage analysis. The stator current for constant voltage analysis is calculated using the characteristics equations (4.1) and (4.2) of PMBL motor. The experimental results are observed to be in close agreement with the analytical results obtained from the isotropic models than anisotropic as depicted in Fig 4.2. This is because the effect of stator slotting is not effective in SMPM motors. With the presence of PM, the total effective air gap turn out to be large as the recoil permeability of PMs used is nearly unity.

The Residue method has been used for predicting the torque-speed characteristics of the motor at two different stator supply voltages using isotropic model and the results obtained from the test motor and analytical model has been shown in Fig 4.3. Theoretical results obtained from the residue method have been validated with the experimental results and are noticed to be in close agreement. The effect of stator slotting in the air gap flux density distribution has been shown in Fig 4.4. It has been observed that FEM results and those obtained from slotted model have a good agrrement thus showing effectivenss and accuracy of the proposed model [Dwivedi *et al.*, 2016]. The Residue method has been further used for the calculation of back-EMF and flux density using isotropic model. The back-EMF computed from the developed model is compared with the back-EMF induced at different speeds in the stator windings obtained using search coils in the test motor and the comparison is shown in Fig 4.5.

Since the proposed method computes the performance of the machine directly from the physical parameters, the effect of change in design parameters on the performance of the motor can be easily predicted. The torque-speed characteristic at various air gap and thickness of PM keeping total *'entrefer'* has been shown in Fig 4.6. The increase in PM height and decrease in air gap, increases the flux and thus increases the output torque of the SMPM machine. However, the air gap cannot be decreased beyond a certain level so as to avoid saturation. The torque-speed characteristics with different types of PMs have been depicted in Fig 4.7. The ferrite PMs offer almost a constant characteristic suitable for applications requiring operation in constant torque region like electric vehicle, conveyers, traction, etc. while the motors with NdFeB PMs are a good choice for pumps, fans, blowers, .i.e., variable load applications. Both NdFeB and Ferrite PMs may be used to develop a variety of applications. The NdFeB magnets with larger airgap is suitable for high speed applications as investigated here.

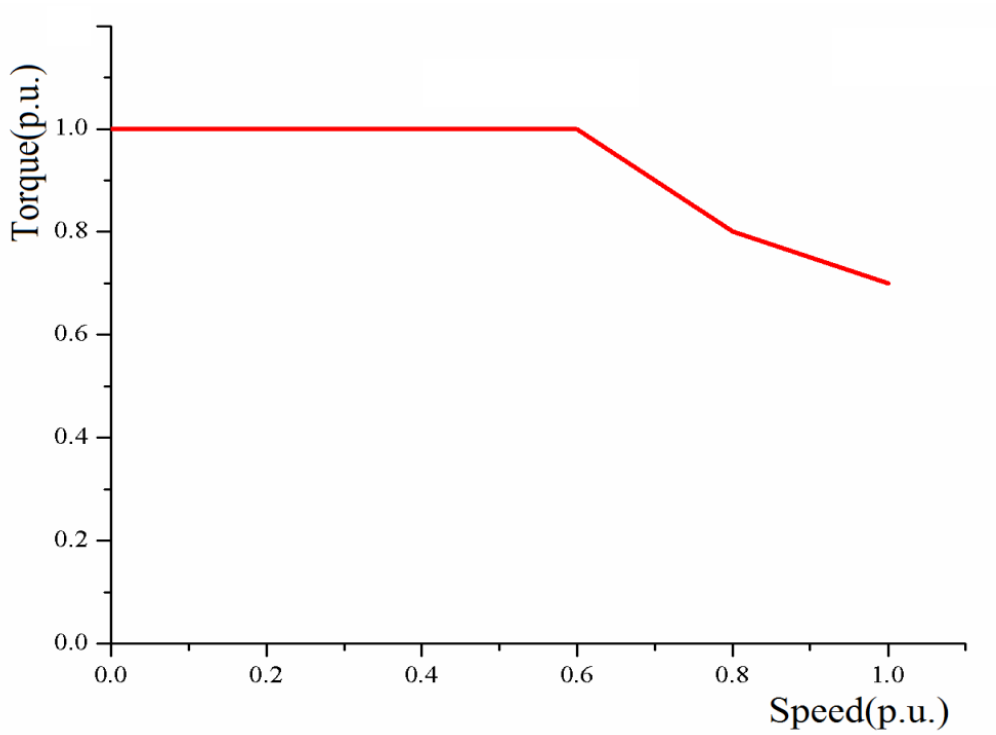

Fig. 4.1 Typical Torque-Speed Characteristics of PM Motor

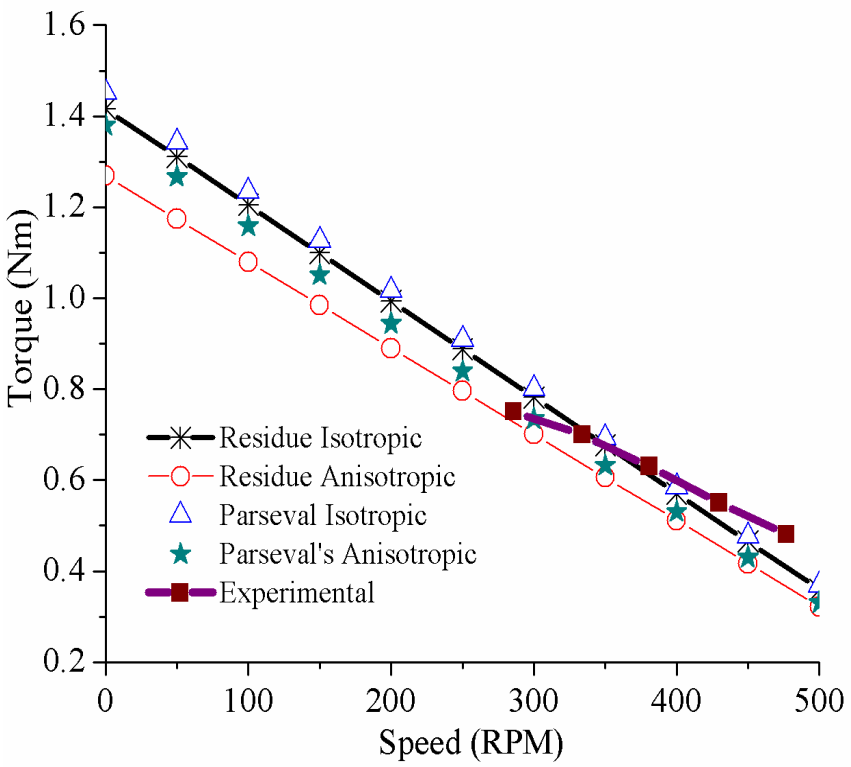

Fig. 4.2 Torque-Speed Characteristics from experimental and analytical calculation at constant voltage at V=30V

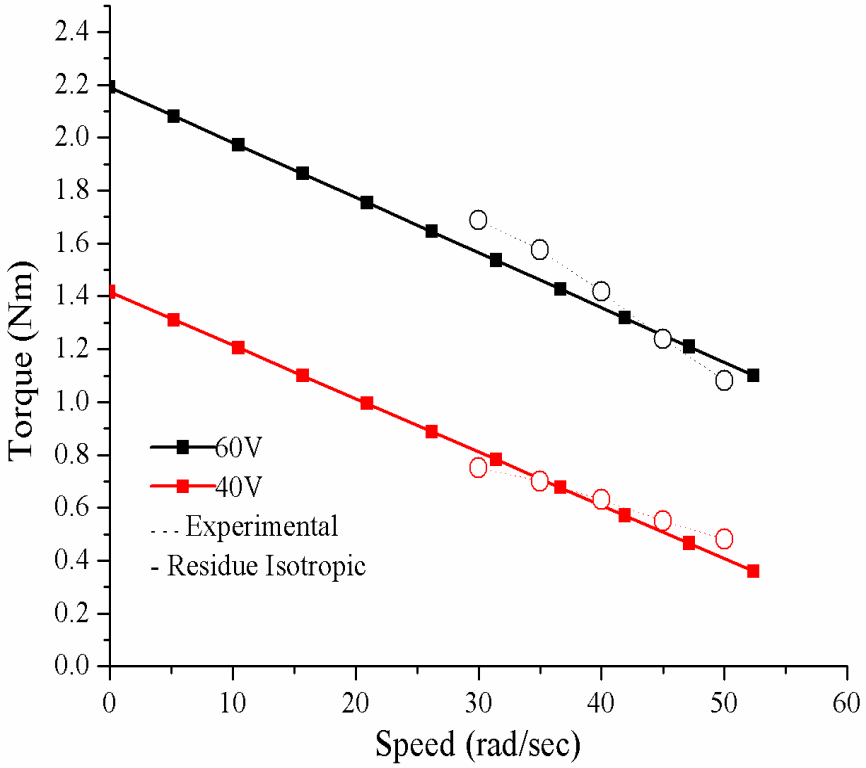

Fig. 4.3 Torque-Speed Characteristics calculated by Residue Theorem at two different stator supply voltages

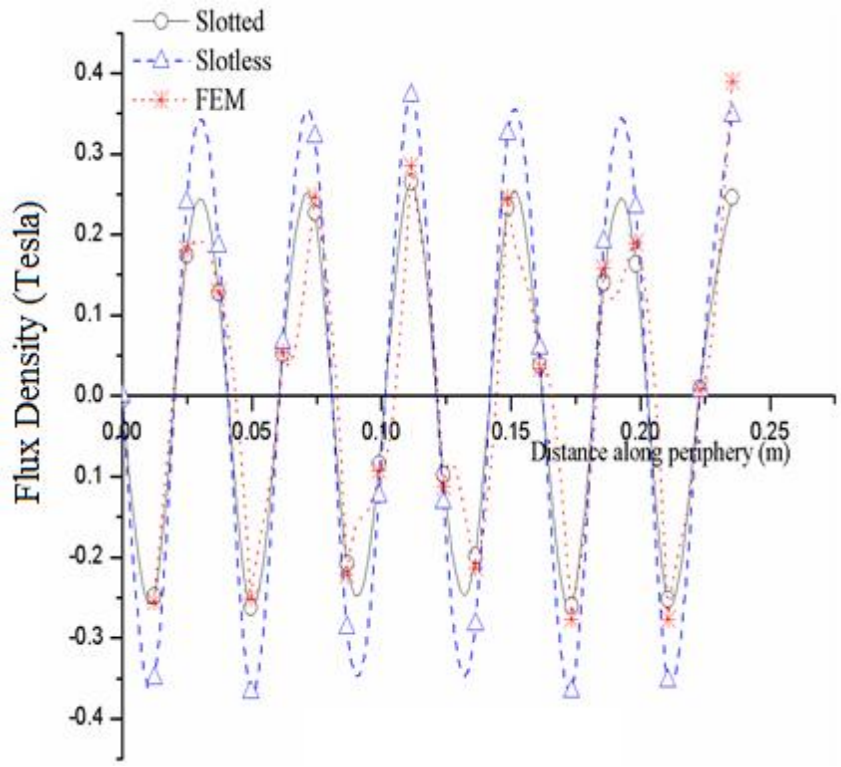

Fig. 4.4 Flux density distribution along air gap with and without slotting effect using Residue Method and its validation by FEM

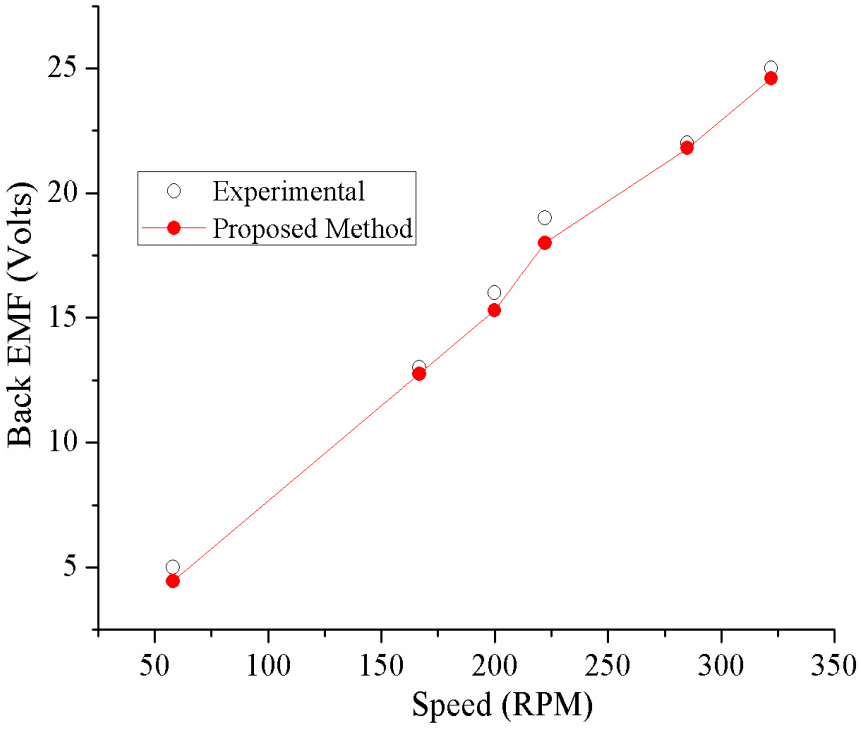

Fig. 4.5 Validation of calculated Back EMF from Residue Method and Experimental Results for Machine-A

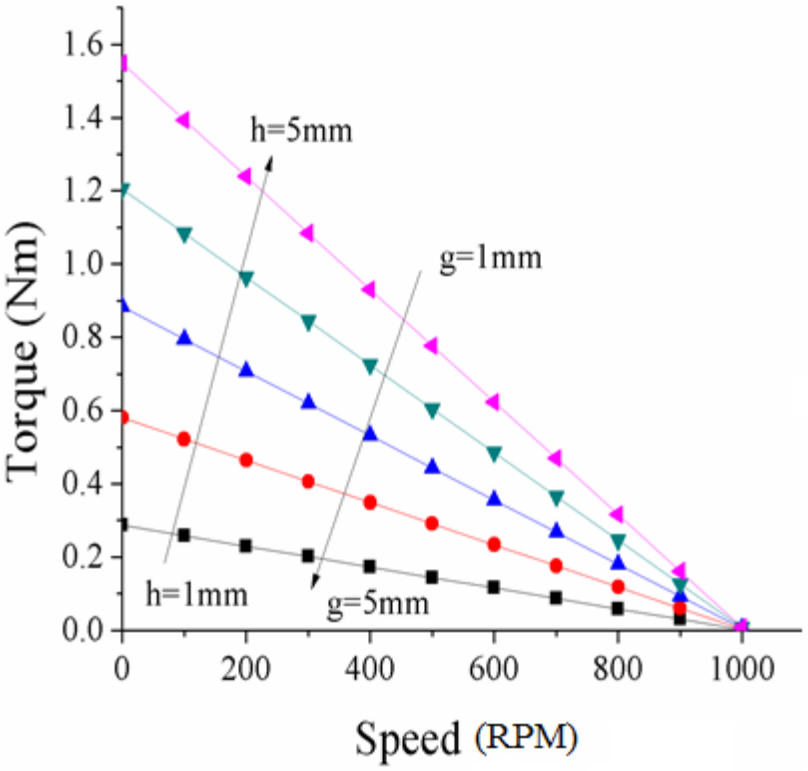

Fig 4.6 Effect of variation of PM thickness and air gap on Torque-Speed Characteristics of Machine-A

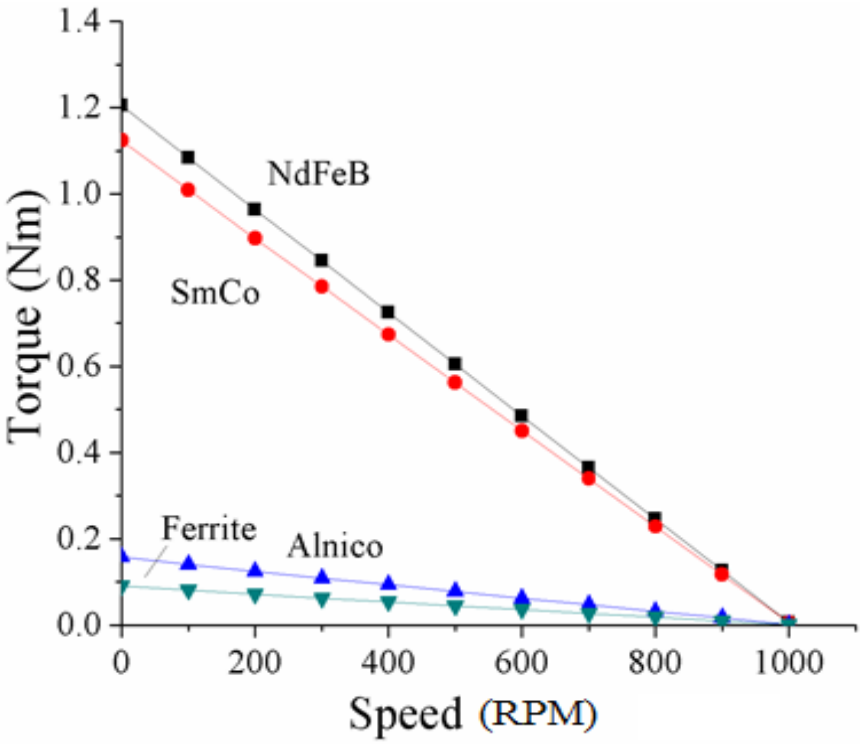

Fig. 4.7 Effect of different of type of PMs on Torque-Speed Characteristics of Machine- A

4.3 AFPM Motor

The experimental results obtained from the three AFPM motors have been compared with that obtained from the analytical method using space Fourier transform. The method is also capable of calculating the performance of the multi-phase fault tolerant motors.

4.3.1 5-phase AFPM Motors: Machine-B and Machine-C

This section reports the validation of the results obtained from the analytical method and the experimentally obtained results. As discussed in Section 2.3.6 that residue theorem seems to be more realistic as such residue theorem has been used for computation. The five-phase AFPM motor can continuously produce torque in the event of loss of one phase or two phase, the motor therefore may be used as Fault tolerant PM motor. The torque-speed characteristics of two 5-phase AFPM motors (Machine-B and Machine-C) have been computed for healthy and faulty conditions. It is expected that the proposed approach can also be used for the analysis of *Fault Tolerant PM Motors.*

The theoretical torque-speed characteristics of Machine-B as motor has been validated with the experimental results as depicted in Fig. 4.8. While Fig. 4.9 and Fig. 4.10 depict the torque-speed characteristics in the event of loss of one or two phases. The results obtained from the test motor and the proposed method depicts a very close agreement. It can be concluded that the proposed method is well suited for calculation of performance of the SMPM motor in the event of fault, thus making it suitable to compute performance of *'Fault Tolerant Applications'*. Since the effective air gap is large, the results calculated from the isotropic and anisotropic model are close to each other. Fig. 4.11 depicts the torque-speed characteristics for the 5-phase 6-pole motor (Machine-C) in healthy condition. The results obtained are validated with that computed using the residue isotropic method. Fig. 4.12 shows the performance of the

motor in the event of fault. The EMF of 6-pole motor at various speeds has also been calculated from the method and has been shown in Fig. 4.13.

4.3.2 3-phase AFPM motor: Machine-D

The fabricated AFPM machine is a slotted stator single sided air gap motor with axial flux sheet induction motor on the other side of the stator to provide the starting torque. The slotted AFPM configuration uses less copper and PM material [Sitapati *et al.*, 2001]. The performance characteristic of the 12-slot 3-phase 4-pole AFPM motor (Machine-D) has been shown in Fig. 4.14 and Fig. 4.15. For AFPM machines, the computation of torque and flux density has been done at average radius of the stator as discussed in Section 2.4, since in AFPM the linear current density is a function of the radius. All the computations are carried out using Residue Theorem since the method gives more close solutions to the experimental results. The results obtained from isotropic and anisotropic model are very close as the air gap of the AFPM motor is large due to mechanical constraints as reported in Section 3.6 making the overall effective air gap high. For lesser air gap, improved fabrication facilities are required which was beyond the scope of the present work. The back-EMF induced in the main winding at different speeds has been shown in Fig. 4.16. The cogging torque of the AFPM motor has also been calculated and validated using experimentally obtained results as shown in Fig. 4.17. For the measurement of cogging torque, the machine is coupled to a DC motor and the PM rotor is set at different angles during start up. At different positions of the rotor w.r.t. a common slot, the cogging torque is measured.

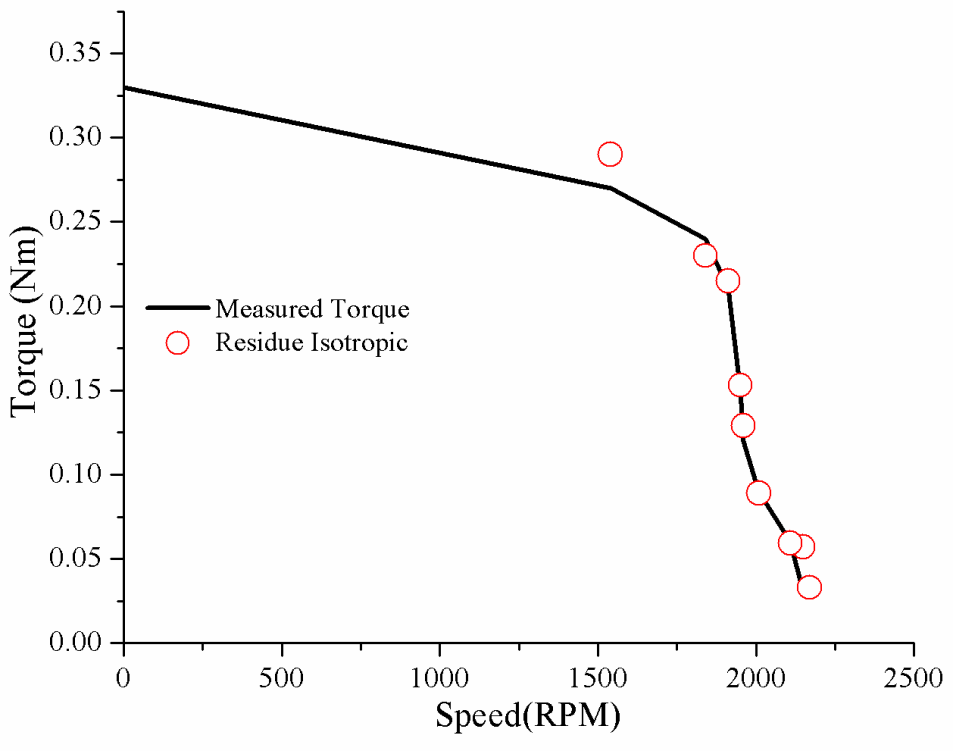

Fig. 4.8 Torque-Speed characteristics of the Machine-B in healthy condition

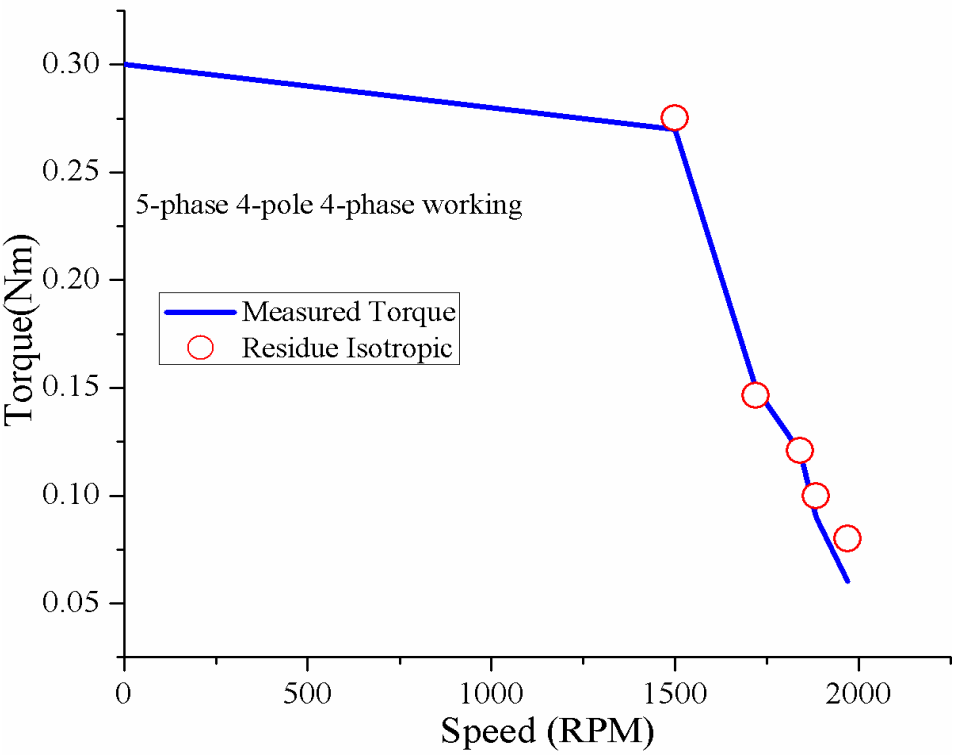

Fig. 4.9 Torque-Speed characteristics of the Machine-B with one faulty phase

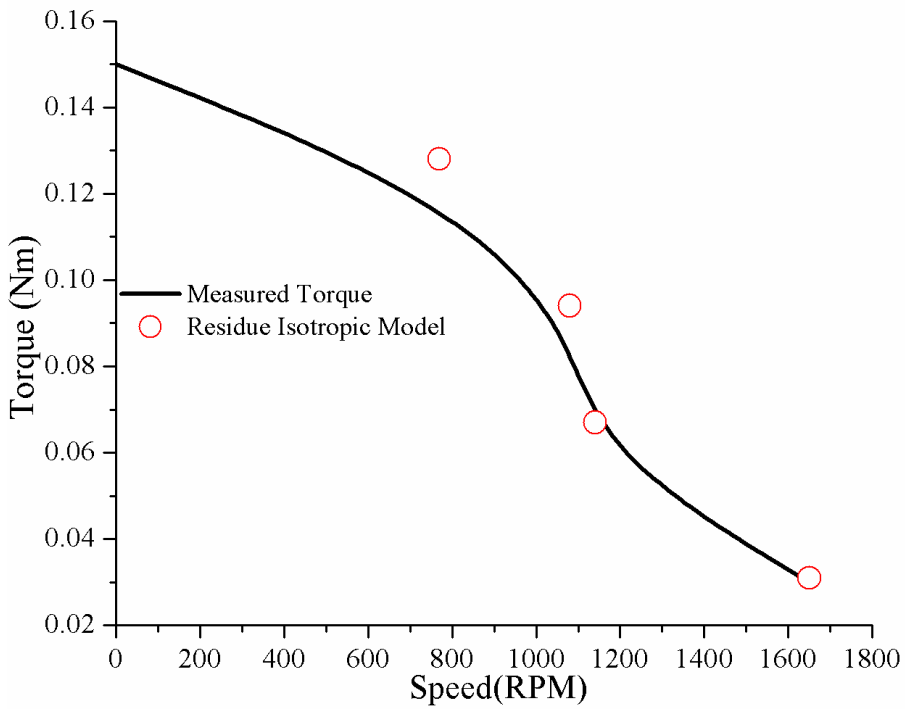

Fig. 4.10 Torque-Speed characteristics of the Machine-B with two faulty phases

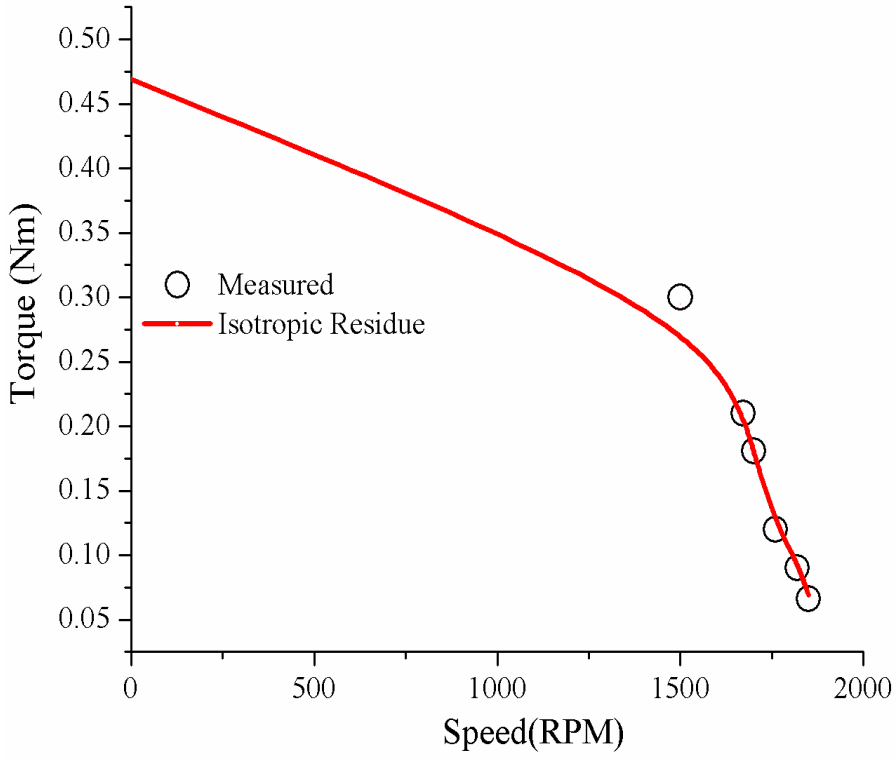

Fig. 4.11 Torque-Speed characteristics of the Machine-C in healthy condition

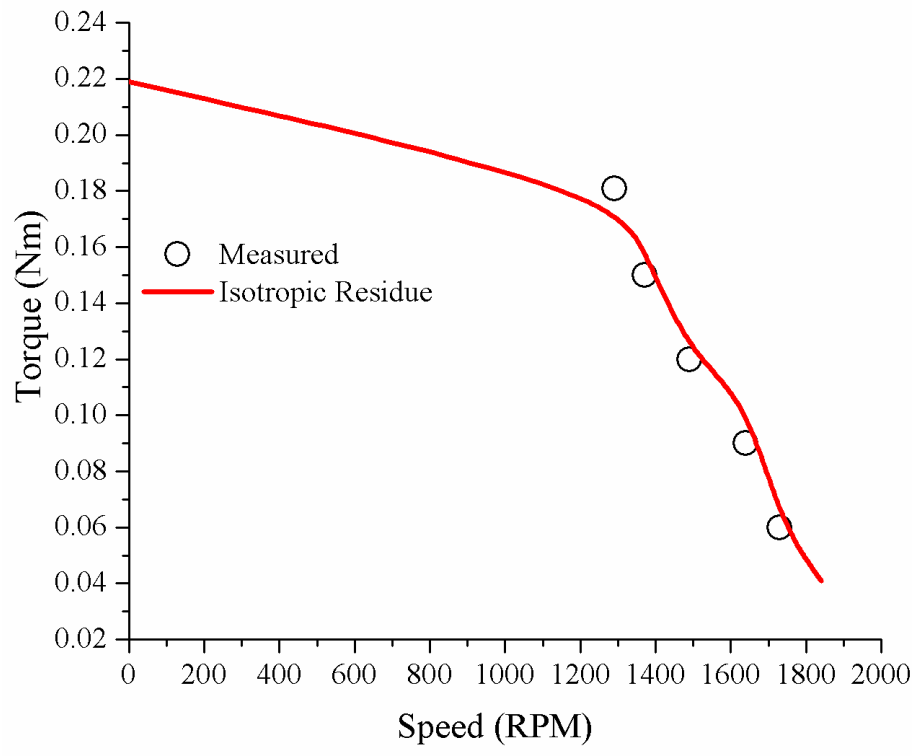

Fig. 4.12 Torque-Speed characteristics of the Machine-C with one faulty phase

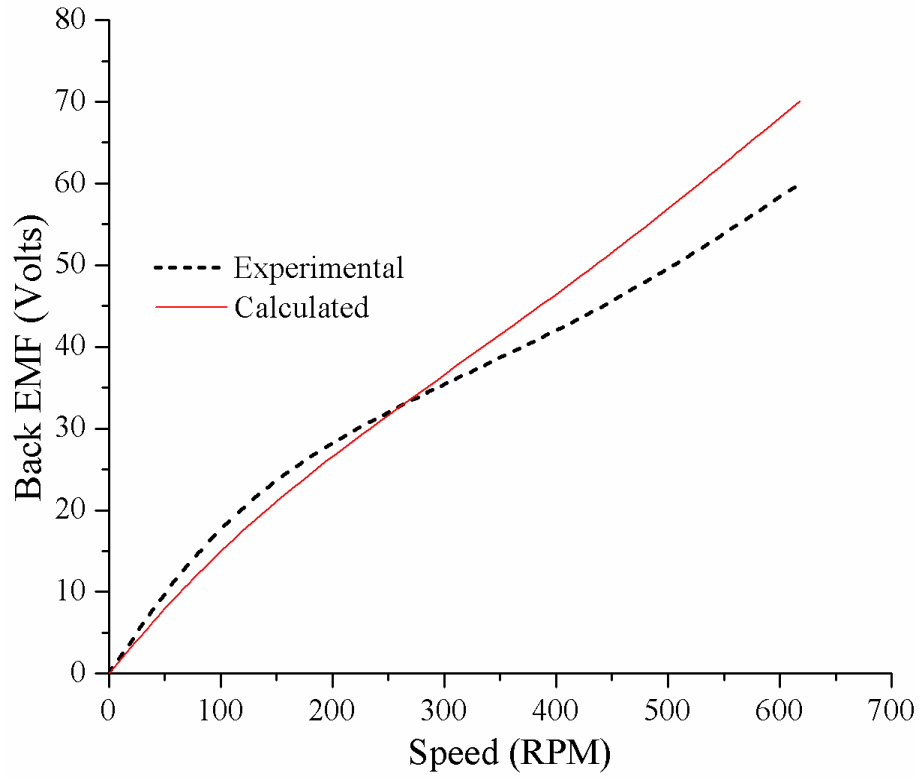

Fig. 4.13 EMF vs Speed for Machine-C

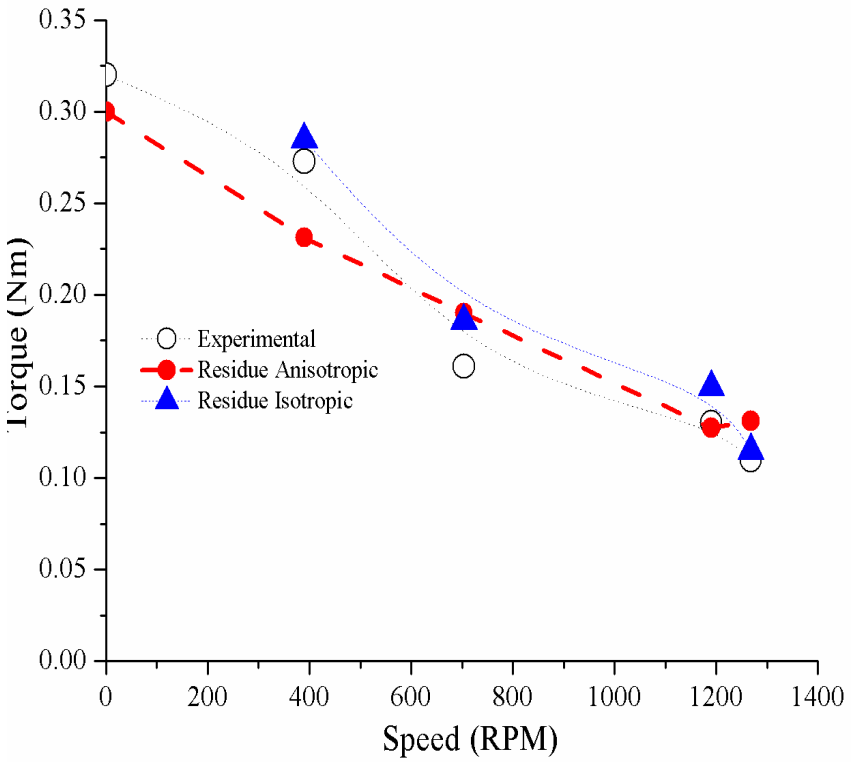

Fig. 4.14 Torque-Speed Characteristics obtained from experimental setup and Residue Method for Machine-D

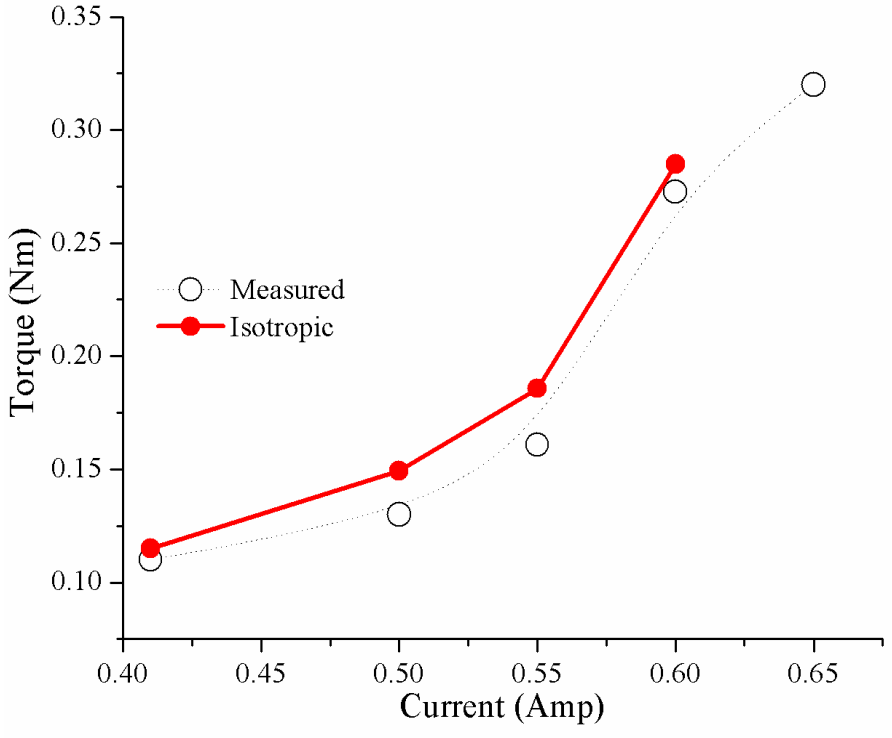

Fig. 4.15 Torque Vs Stator Current Characteristics for Machine-D

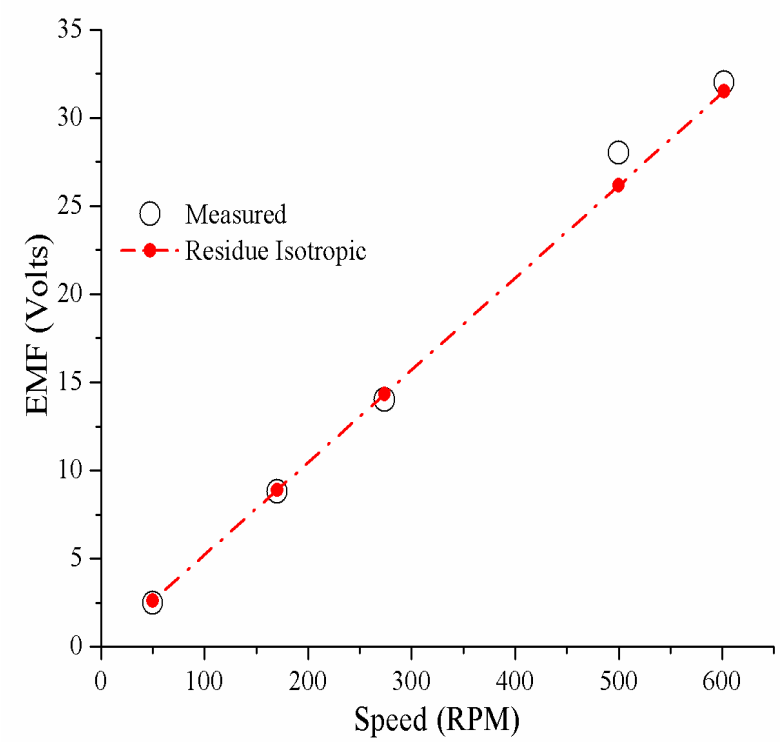

Fig. 4.16 Comparison of EMF induced at different speeds and calculated from the Residue Method for Machine-D

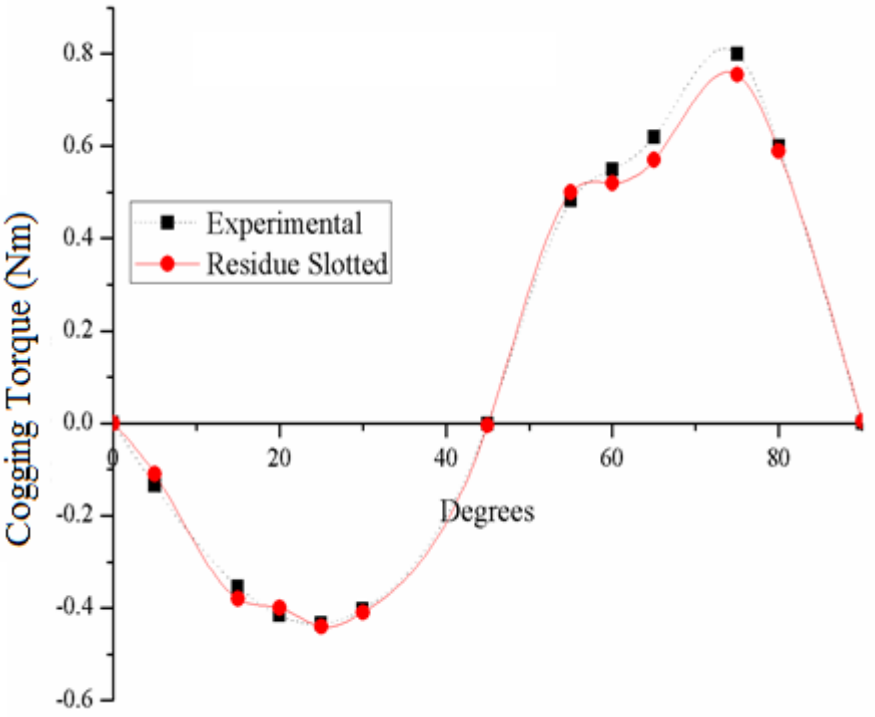

Fig. 4.17 Variation of cogging torque with angular displacement for Machine-D

4.4 Analytical Validation and Comparison of Methods of Analysis

Along with the experimental validation of the proposed method in the previous section, this section presents analytical validation of the proposed method from different methods. The torque-speed characteristics for Machine A as a motor has been computed using analytical methods and depicted in Fig. 4.18. The percentage error from the characteristics obtained from experimental results has been reportedly more when conventional method is applied compared to MEC and Fourier series methods. However, the Fourier transform gives the minimum error. The effect of stator slotting has been included using the anisotropic models, however, since the air gap of the experimental RFPM motor is large, the experimental results obtained are more close to isotropic characteristics. Fig. 4.19 depicts the torque-speed characteristics of Machine-B and the experimental results obtained from the Fourier transform and dq0 model has been compared. A close agreement has been observed from the results. Both the methods are competitive and showing results close to the measured values.

Fig. 4.20 shows the variation of output torque with the input stator current obtained from the Machine-B and calculated from different analytical methods. The Fourier transform shows a good agreement with the experimental results at all the input currents and is concluded to be a better analytical option. The magnetic flux distribution in the air gap computed from above methods has been shown in Fig. 4.21. The performance prediction of PM motor from MEC method involves rigorous calculations and is time consuming. While the conventional methods are suitable when the air gap of the machine is large and the effect of saturation needs not be included. The computation time of Fourier series method is dependent on the speed of the machine and as the speed of the motor increases, the computation time also increases. In contrast to all the methods compared, the Fourier transform method has been proved to be more realistic

and provides accurate results with lesser computational time. Moreover, the proposed method involves no discretization of geometry and the performance can be directly computed form the physical dimensions of the machine.

4.5 Fault Tolerant Characteristics of 5-phase AFPM motor

This Section represents the fault tolerant characteristics of the AFPM machines developed. Since, interest in permanent magnet synchronous machines for safety-critical applications has been increasing over the years, the most common methods for providing fault tolerance to a PM machine is to provide fault tolerance to each component of the machine-either the driving circuit or the machine itself. This requires designing machines with the lowest possible mutual coupling between phases and a high self-inductance. The concentrated windings provide less mutual coupling between phases and also increases self-inductance of the windings for limiting the short-circuit current. The prototype 10-slot 5-phase AFPM machine uses concentrated windings along with PM Enhanced sensing scheme using shadow coil as control scheme. Since the scheme uses separate amplifiers for each phase, in case of fault if one of the phase or amplifiers become faulty, the other phases will remain unaffected and the motor will work continuously. The loss in torque or speed may be compensated by increasing the bias voltage to the healthy phases. This calls for embedded technologies such as d-SPACE and FPGA. This is the main requirement of the Fault tolerant motors for safety critical applications which requires continuous operation. Fig. 4.22 and Fig. 4.23 shows the performance of the AFPM motors in healthy and faulty condition. In the event of fault, when some of the phases are not working, the total current reduces and the motor works with reduced torque and speed.

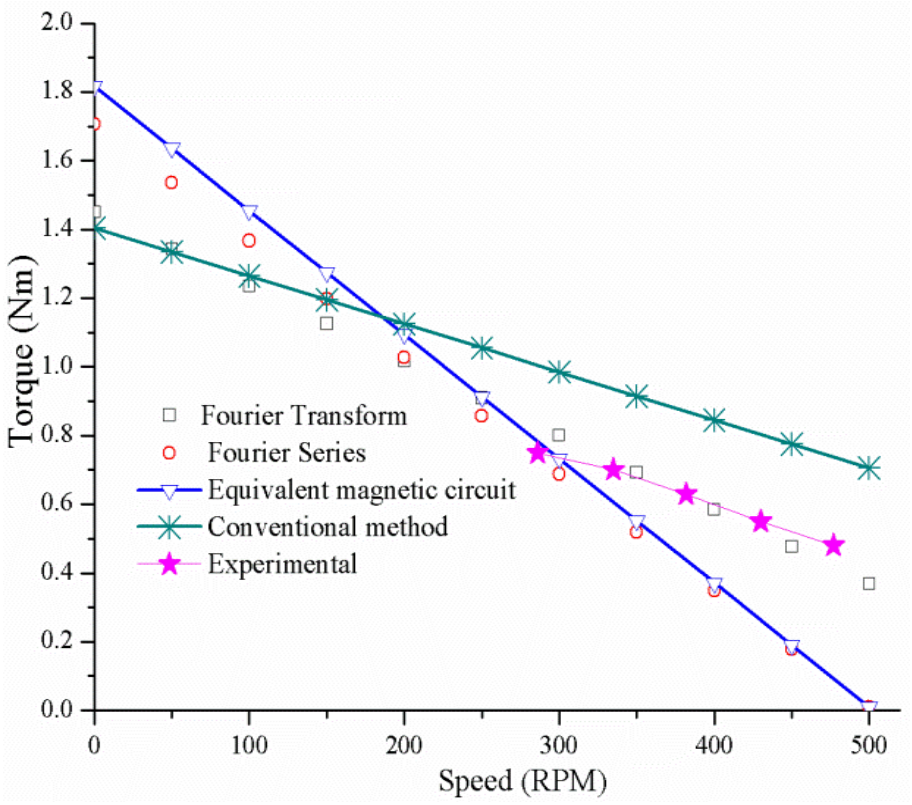

Fig. 4.18 Torque-speed characteristics for RFPM motor- Machine-A obtained from various methods and its validation with experimental results

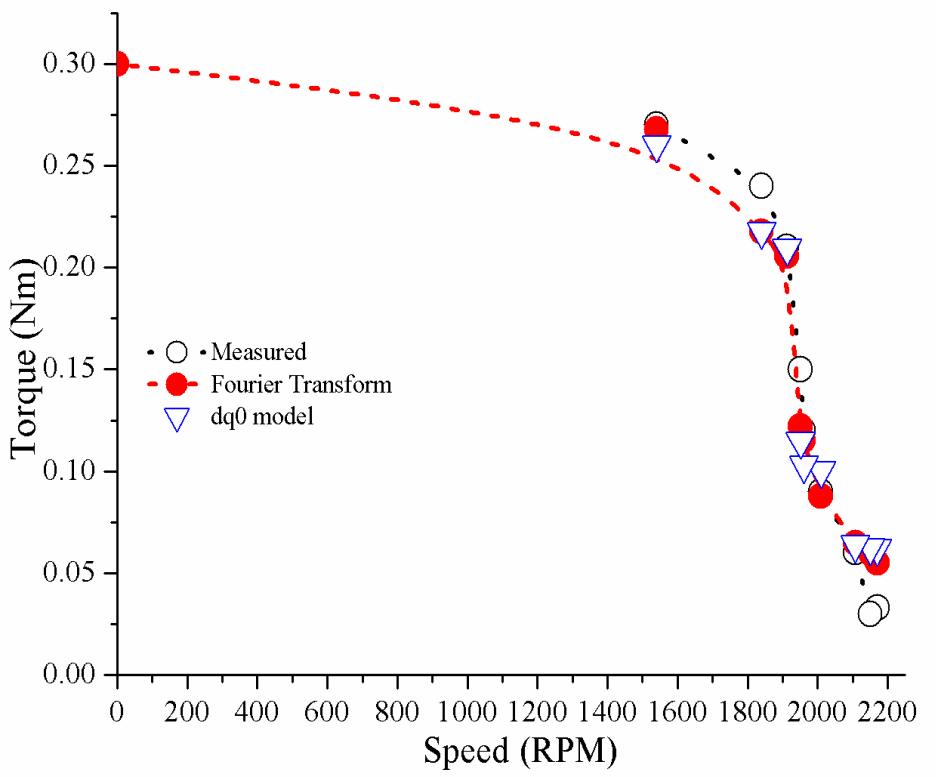

Fig. 4.19 Torque-speed characteristics of Machine-B

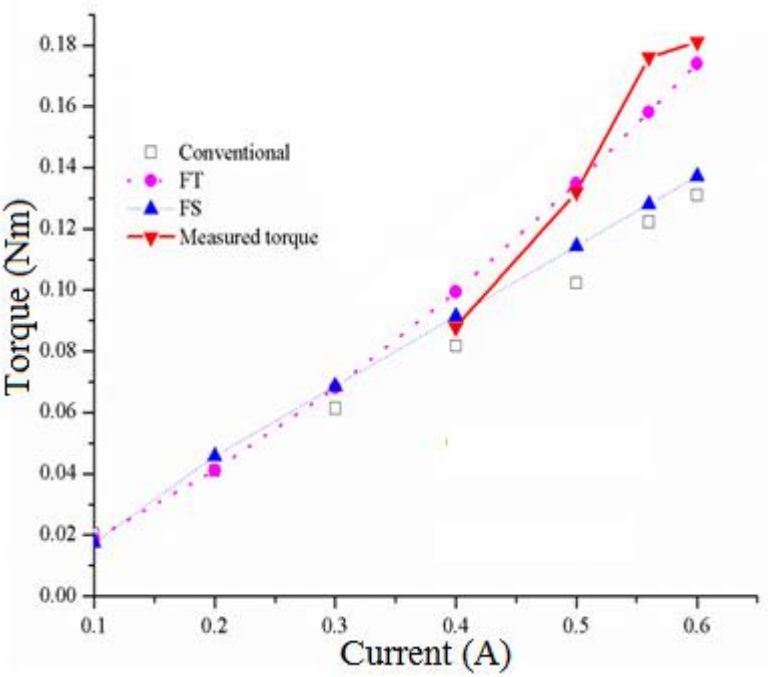

Fig. 4.20 Torque-Current characteristics calculated by different analytical methods for Machine-B

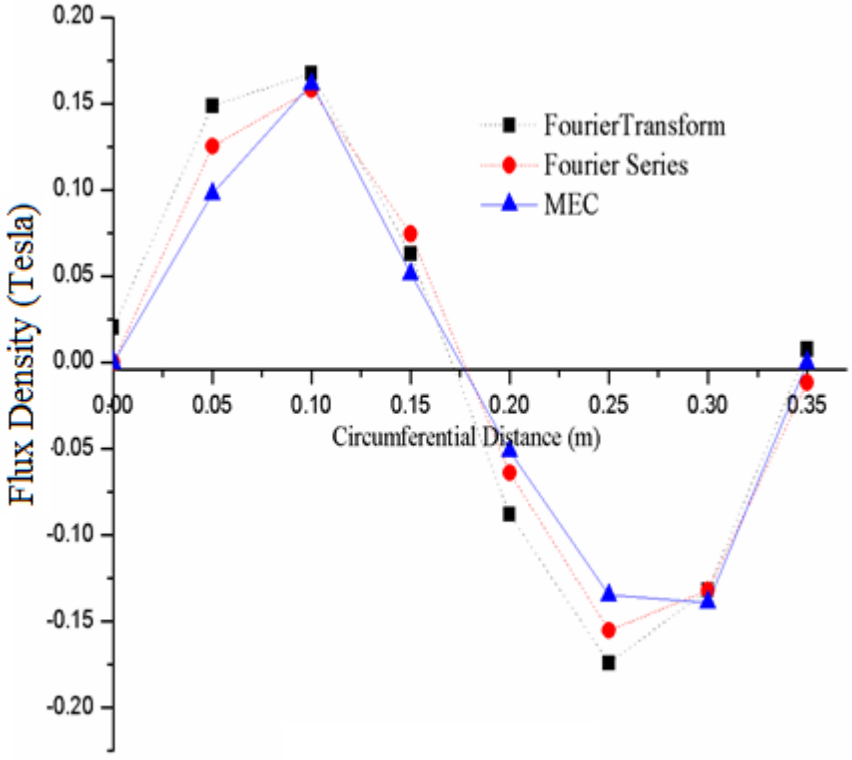

Fig. 4.21 Air gap flux density comparison obtained for Machine-B

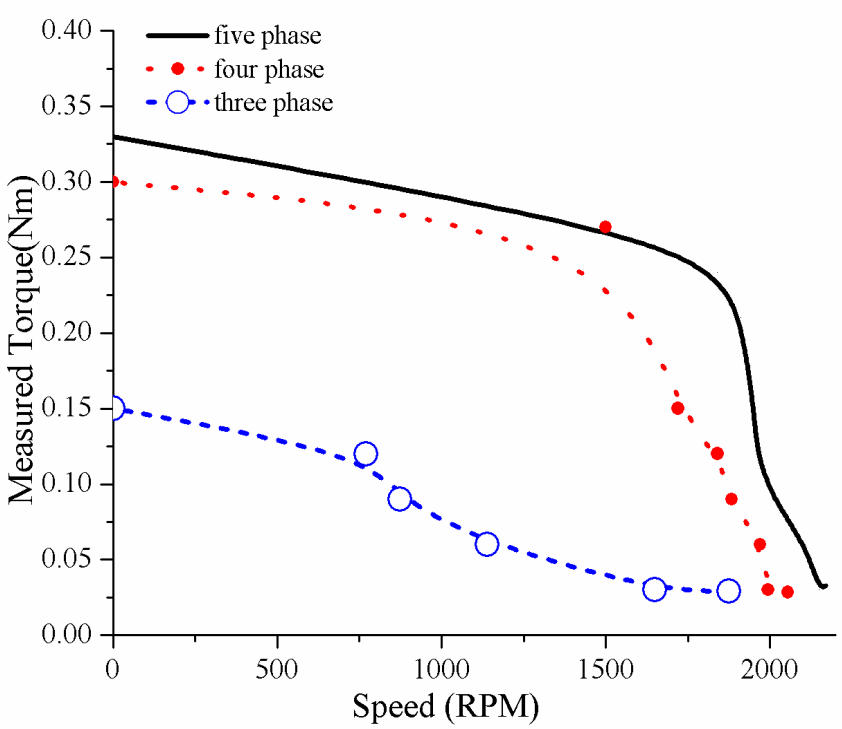

Fig. 4.22 Torque-Speed Characteristics of Machine-B under healthy and faulty condition

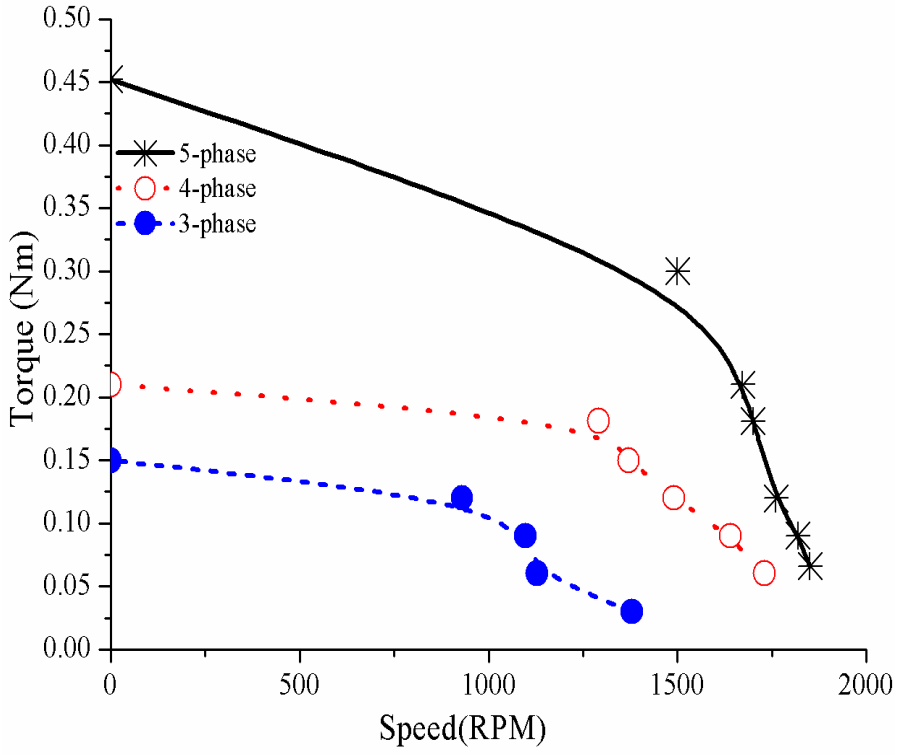

Fig. 4.23 Torque-Speed Characteristics of Machine-C under healthy and faulty condition

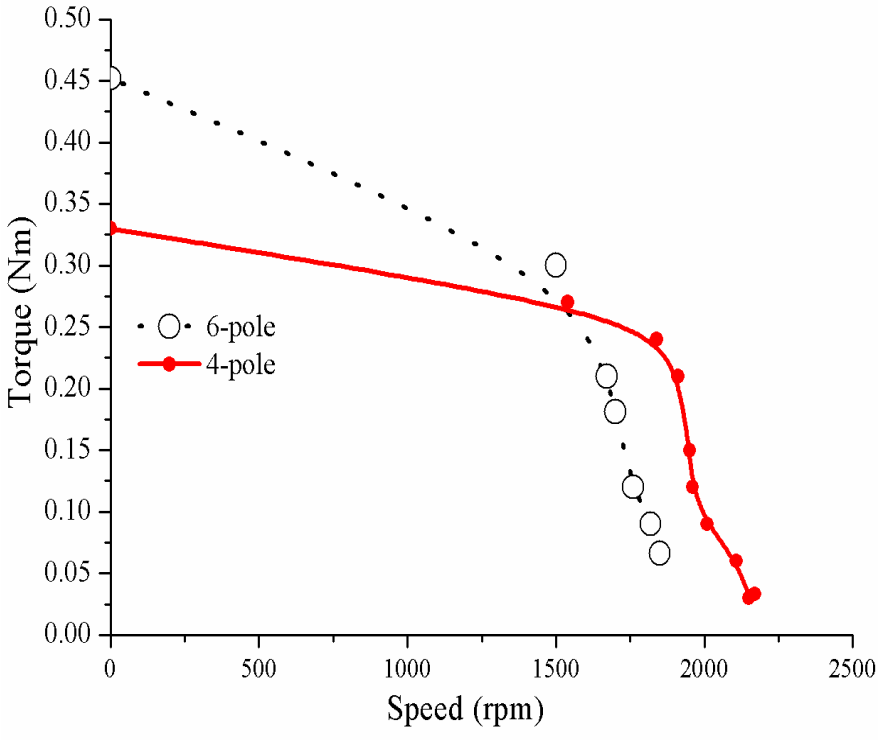

Fig. 4.24 Performance Comparison of five phase AFPM motors

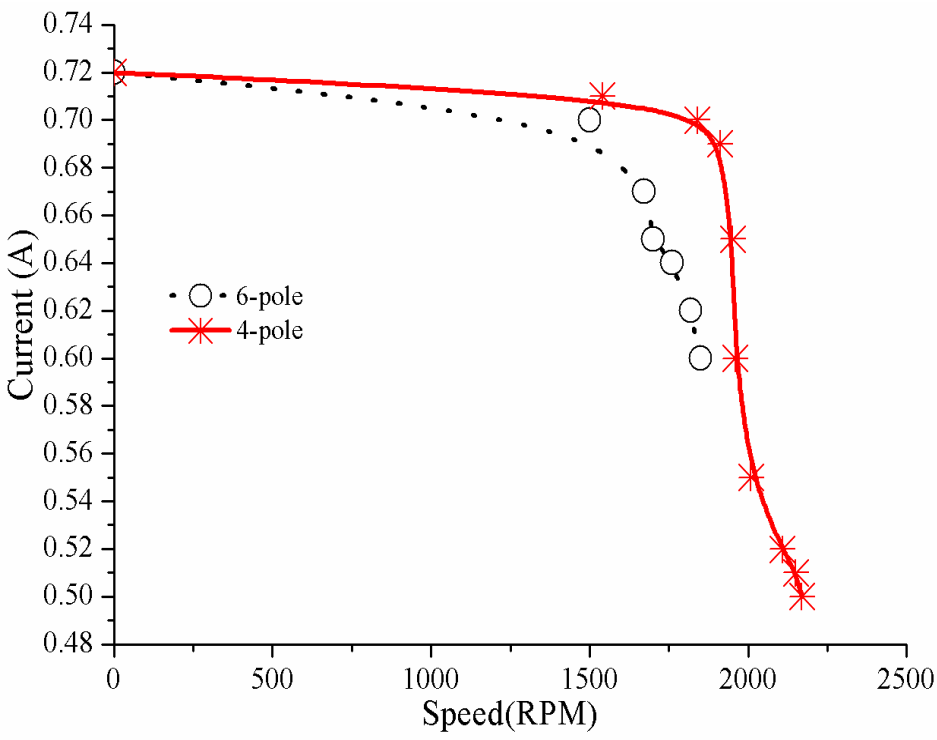

Fig. 4.25 Current Vs Speed variation of 5-phase AFPM motors

The performance during fault condition is determined using concept of symmetrical components. There exist two current sheets each for forward and backward rotating magnetic fields. The maximum torque for 4-pole AFPM motor when machine was running with all the phases working is 0.33 Nm. In the event of loss of one phase, the maximum torque reduces to 0.3 Nm, however when fault occurs in two phases the torque drops to 0.15 Nm.

For 6-pole AFPM motor, the maximum torque is 0.46 Nm. The torque reduces to 0.22 Nm in the event of loss of one phase and to 0.15 Nm when fault occurs in two-phases. The maximum torque of the machine is less because of the large air gap of 10 mm in the motor due to mechanical constraints. It can be concluded from the figure that constant power region of the motor increases during faults.

Table 4.1 Maximum Ratings of the AFPM Motors

	5-phase 4-pole	**5-phase 6-pole**	**3-phase 4-pole**
Efficiency	89.27%	91.7%	73.2%
Torque	0.33 Nm (semi-closed slots)	0.47 Nm (semi-closed slots)	0.33 Nm (open slots)
Power	450 Watts	441 Watts	450 Watts

Fig. 4.24 shows the performance comparison of two 5-phase AFPM motors developed. The machine with larger number of poles has short constant torque region but high rated torque while machine with less number of poles has comparatively lesser rated torque. This is due to the increase in air gap flux density with the number of poles.

Fig. 4.25 depicts the variation of speed with the phase current in the two five phase AFPM motors and motor with larger number of poles is reported to have less operating current. Table 4.1 gives the maximum ratings of the AFPM motors at the air gap of about 10 mm. However, if the air gap is reduced to a minimum of 1 mm, the flux density in the air gap increases and thus, the torque, efficiency and output power delivered will increase. The capacity of machine is expected to be high for lesser air gap and larger bias voltage.

4.7 Summary and Conclusions

The experimental results obtained from the RFSMPM and AFSMPM motors are compared with that obtained from the proposed analytical method. The performance characteristics, back-EMF induced in the motor windings, flux density and cogging torque has been calculated and validated by the proposed method. The results also show that the method can be used effectively for the analysis of fault tolerant PM motors. The fault tolerant studies of the two 5-phase motors have also been completed. The results computed from proposed method show good agreement with the experimental results. The method also proved to be a good candidate for the performance analysis of fault tolerant motors. With the presence of large air gap, the air gap flux density is less and thus, the total torque produced is also less. To improve the performance of these motors, the provision of less air gap with proper fitting arrangements has to be made. The next Chapter presents summary of contributions and results presented by this thesis work. Suggestions for further work to extend the thesis work will also be discussed.